

## Soil Water Storage and Active-layer Development in a Sub-alpine Tundra Hillslope, Southern Yukon Territory, Canada

W. L. Quinton,<sup>1\*</sup> T. Shirazi,<sup>1</sup> S. K. Carey<sup>2</sup> and J. W. Pomeroy<sup>3</sup>

<sup>1</sup> Simon Fraser University, Burnaby BC, Canada

<sup>2</sup> Carleton University, Ottawa, Ontario, Canada

<sup>3</sup> Centre for Hydrology, University of Saskatchewan, Saskatoon, Canada

### ABSTRACT

Estimates of water flux and storage in organic-covered, permafrost terrains require an understanding of the factors controlling soil thaw. Field studies conducted in southern Yukon Territory, Canada, showed that ground freezing and thawing commenced at temperatures between  $-0.14$  and  $-0.24^{\circ}\text{C}$ . A temperature drop below  $-0.6^{\circ}\text{C}$  had little effect on unfrozen moisture content. Unfrozen moisture storage shifted abruptly between a winter period value of *ca.* 50 mm and a summer period value of *ca.* 100 mm, although soil temperatures remained close to the freezing point for extended periods. The organic soil transmitted water laterally early in the thaw period while the water table still remained in the organic soil. Following this period, water movement was mainly vertical, between the ground surface and the underlying mineral sediment. The cumulative energy consumed in melting ice ( $\Sigma Q_i$ ) in the active layer was *ca.* 76% of the cumulative ground heat flux, and *ca.* 15% of the cumulative net all-wave radiation ( $\Sigma Q^*$ ) measured over the snow-free ground surface. A strong linear correlation between  $\Sigma Q^*$  and  $\Sigma Q_i$ , suggests that the degree of soil thaw can be estimated from  $\Sigma Q^*$ . Copyright © 2005 John Wiley & Sons, Ltd.

KEY WORDS: organic soils; permafrost; soil moisture; sub-alpine

### INTRODUCTION

Organic-covered permafrost terrain occupies much of the circumpolar region (Bliss and Matveyeva, 1992). In these areas, the storage and flow of water within the active layer are strongly controlled not only by the presence of permafrost and seasonally frozen ground, but by soil profiles with thick organic surface horizons (Quinton and Marsh, 1999; Carey and Woo, 2001). The infiltration, storage and redistribution of water below the ground are complex due to phase changes, depth-variations in soil transmission properties, and

spatial and temporal variations in the elevation of the frost table (Gray *et al.*, 2001; Carey and Woo, 2001; Spence and Woo, 2003; Hayashi *et al.*, 2004). Soil moisture variability and state also affect summer evaporation and therefore the recycling of water within drainage basins (Granger and Pomeroy, 1997). This subsequently exerts a primary control on infiltration into frozen soils during the spring (Gray *et al.*, 2001; Janowicz *et al.*, 2003). Northern areas are expected to undergo the greatest degree of warming over coming decades (Comiso and Parkinson, 2004; IPCC, 1996). Physically-based, numerical models are needed to predict the flux and storage of water in these regions.

In many northern, organic-covered terrains, the ground is saturated, or nearly saturated with ice and a small amount of unfrozen water, at the onset of snowmelt runoff in the spring (Quinton and Gray,

\* Correspondence to: W. L. Quinton, Department of Geography and Environmental Studies, Wilfrid Laurier University, Waterloo, Ontario, Canada N2L 3C5.  
E-mail: wquinton@wlu.ca

Received 15 September 2004

Revised 3 July 2005

Accepted 5 August 2005

2001). The upper surface of the frozen, saturated soil is relatively impermeable to infiltrating meltwater and, when the ground is thawing, this surface coincides closely with the zero-degree isotherm (i.e. frost table) (Carey and Woo, 1998; Quinton *et al.*, 2000). Since the saturated, horizontal hydraulic conductivity,  $k_s$ , decreases exponentially with depth (Quinton and Gray, 2003; Carey and Quinton, 2005), the depth of the relatively impermeable frost table is critically important in controlling the rate of subsurface drainage from hillslopes. Proper estimation of this flux therefore requires that the depth of thaw be known, so that an appropriate value of  $k_s$  can be assigned.

The objectives of this paper are to a) examine the effects of soil freezing and thawing on the unfrozen moisture content of the organic soil cover, b) measure the ground heat flux, including the energy consumed in melting ice in the active-layer, and c) recommend a method of estimating active-layer development during snow ablation and ground thawing.

## STUDY SITE

The study was conducted in Granger Creek (60° 32' N, 135° 18' W), located within the Wolf Creek Research Basin, 15 km south of Whitehorse, Yukon Territory, Canada, during 2002 and 2003. The area has a subarctic continental climate characterized by a large temperature range and low precipitation. Mean annual January and July temperatures from the Whitehorse airport (elevation 706 m a.s.l.) are -17.7°C and +14.1°C. Mean annual precipitation is 267 mm, of which 122 mm falls as snow (1971–2000). Precipitation at the Whitehorse airport may underestimate basin precipitation by *ca.* 25 to 35% (Pomeroy and Granger, 1999). The Granger Creek drainage basin is *ca.* 8 km<sup>2</sup> in area and ranges in elevation from 1310 m to 2250 m a.s.l. The main river valley trends west to east at lower elevations, resulting in predominantly north- and south-facing slopes. Permafrost occurs under much of the north-facing slopes and at higher elevations, whereas seasonal frost predominates on southerly exposures.

Throughout the basin, the ground cover is composed of a continuous cover of sphagnum moss and various herbs, including Labrador tea (*Ledum* sp.), sedges, grasses and lichens. Some woody vegetation is present, including willow shrubs (*Salix* sp.), and a few scattered spruce (*Picea* sp.) trees. Willow and birch shrubs, 2–3 m in height occupy much of the channel and riparian zones. They also extend upslope but decrease in density and height. In the mid-slope

region, the shrubs are 0.5 to 1 m high and scattered, and at the upper slope, only occasional patches of short (<0.5 m) shrubs occur. A few scattered white spruce (*Picea glauca*) occur within the basin, which is considered above treeline.

The study was conducted near the outlet of Granger Creek on a 17.5° north-facing slope that is underlain by a 15 to 20 m thick permafrost layer (Pomeroy and Granger, 1999). The length of the slope from its crest to the streambank is approximately 150 m. Each year, a deep (>2 m) snow drift forms on the upper part of the slope, and persists for 3 to 4 weeks after the disappearance of the surrounding snow cover. The thickness of the organic soil decreases with distance upslope from *ca.* 0.4 m in the valley bottom to *ca.* 0.08 m near the crest.

Overland flow was not observed anywhere on the hillslope during the study, and hillslope runoff was therefore conveyed through the active layer, the maximum thickness of which ranged between *ca.* 0.4 m on the slope crest to >1 m near the slope base. At the time the ground surface becomes snow-free on the study slope, the relatively impermeable frost table is typically within the upper 0–0.05 m depth range. It then descends through the soil profile as the active layer thaws. Average saturated, horizontal hydraulic conductivity values of the organic soil were measured by tracer tests. These values decreased from *ca.* 40 m d<sup>-1</sup> at 0.1 m below the ground surface to *ca.* 0.85 m d<sup>-1</sup> at 0.3 m depth (Quinton and Gray, 2003).

The underlying mineral sediment had about 31% of particles (by weight) with a diameter of less than 2.00 mm. For the <2.00 mm diameter fraction, the sediment was composed of 57.8% sand (<2.00 > 0.053 mm), 33.8% silt (<0.053 > 0.002 mm), 8.5% clay (<0.002 mm), giving a textural description of sandy loam. The largest measured size range was 37.5–75.0 mm (*ca.* 10% of sample by weight), however 18% of the sample weight was composed of sediment of a larger diameter. The average hydraulic conductivity of the mineral sediment determined by falling water level tests (Bouwer, 1989) was about 0.5 m d<sup>-1</sup> (Quinton *et al.*, 2004), however, where the mineral sediment contained high proportion of coarser grains, hydraulic conductivities as high as 20 m d<sup>-1</sup> were measured.

## METHODOLOGY

In August, 2001, volumetric soil moisture (Campbell CS615, accuracy +/-3%) and soil temperature (Campbell 107B, accuracy +/-0.2°C) sensors were installed at 0.02, 0.05, 0.10, 0.20, 0.30 and 0.40 m

below the ground surface in a pit excavated approximately 100 m upslope of the stream channel. The single pit was assumed to represent the ground thermal regime of the hillslope owing to the very low variation in slope angle, sky view, surface albedo, and organic soil properties (Pomeroy *et al.*, 2003). The 0.34 m deep profile contained two organic layers: i) an upper 0.15 m thick layer composed of living and lightly decomposed, fibric peat, and ii) a lower 0.19 m thick layer composed of sylvic peat containing dark, woody material, and the remains of mosses, lichen and rootlets. The lowest 0.06 m was mineral sediment.

The porosity and bulk density of the organic soil was measured from the method of Boelter (1972), using volumetric soil samples taken from the face of the pit at each depth where moisture and temperature sensors were located. Volumetric soil moisture of these samples was measured, and the results used to calibrate the moisture sensors. This was because the CS615 readings are questionable without a soil-specific calibration (Seyfried and Murdock, 2001). A four-point linear calibration ( $R^2=0.98$ ) was developed covering a volumetric soil moisture range of between 0.4 and 0.7:

$$\theta = 0.5847p - 0.34 \quad (1)$$

where  $\theta$  is the volumetric soil moisture and  $p$  is the measured travel time (milliseconds) of the electromagnetic waves propagating along the wave guide. For soil moistures below 0.4, equation (1) estimates soil moisture values close to the standard response curve provided by the manufacturer. The water table position was monitored continuously in a stilling well installed next to the sensors in the soil pit.

The volumetric heat capacity was calculated from the product of bulk density and specific heat, with values of the latter obtained from the literature (Table 1). The composite volumetric heat capacity of each soil layer was computed from the constituent volumetric heat capacities using equations (2), (3), or (4) defined below. Equation (2) was used if the soil layer was unsaturated and unfrozen, equation (3) if it was saturated and frozen, and equation (4) if it was saturated and unfrozen:

$$Cv_{WSA} = Cv_W\theta + C_S(1 - \phi) + Cv_A(\phi - \theta) \quad (2)$$

$$Cv_{IWS} = Cv_I(\phi - \theta) + Cv_W\theta + Cv_S(1 - \phi) \quad (3)$$

$$Cv_{WS} = Cv_W\theta + Cv_S(1 - \phi) \quad (4)$$

where  $Cv$  is the volumetric heat capacity,  $\theta$  is the volumetric soil moisture content,  $\phi$  is the porosity, and the subscripts  $W$ ,  $S$ ,  $A$  and  $I$  refer to water, soil, air and ice constituents, respectively. An unsaturated and frozen condition did not occur at the measurement depths, and therefore the value of  $Cv$  for this condition was not computed. The thermal conductivity,  $\lambda$ , was computed using the equations provided by Farouki (1981). For the saturated, unfrozen ( $\lambda_{WS}$ ) condition,  $\lambda$  was computed from:

$$\lambda_{WS} = \lambda_w a^2 + \lambda_s(1 - a)^2 + \{\lambda_s \lambda_w (2a - 2a^2) / [\lambda_s(a) + \lambda_w(1 - a)]\} \quad (5)$$

For the saturated, frozen case,  $\lambda_w$  in equation (5) was replaced with the thermal conductivity of ice,  $\lambda_I$ . For the unfrozen, unsaturated condition ( $\lambda_{WSA}$ ),  $\lambda$  was computed from:

Table 1 Volumetric composition of soils and thermal properties used for computations. For each depth increment, the type of organic layer (i.e. u = upper; l = lower) is identified.

Soil type	Sensor/sample depth m	Depth m	Porosity $\phi$ —	Density $\rho$ kg m <sup>-3</sup>	Specific heat* $C$ J kg <sup>-1</sup> K <sup>-1</sup>	Heat capacity $C$ J m <sup>-3</sup> K <sup>-1</sup>	Thermal cond. <sup>†</sup> $\kappa$ W m <sup>-1</sup> K <sup>-1</sup>
org-u	0.02	0.00–0.03	0.94	39.8	1920	76 416	0.21
org-u	0.05	0.03–0.07	0.94	68.3	1920	131 136	0.21
org-u	0.10	0.07–0.15	0.92	80.5	1920	154 560	0.21
org-l	0.20	0.15–0.25	0.85	141.3	1920	271 296	0.21
org-l	0.30	0.25–0.35	0.75	289.8	1920	556 416	0.21
min.	0.40	0.35–0.45	0.49	1104	890	1157 000	2.50
Air	—	—	—	1.2	1010	1 212	0.025
Ice	—	—	—	920	2120	1 950 400	2.24
Water	—	—	—	1000	4185	4 185 000	0.57

Thermal properties are for the soil phase. Values from \*Oke (1987) and †Andersland and Ladanyi (1994).

$$\lambda_{WSA} = (x_w \lambda_w + F_a x_a \lambda_a + F_s x_s \lambda_s) / (x_w + F_a x_a + F_s x_s) \quad (6)$$

where  $a$ , a function of porosity, is calculated from the soil porosity using formulae provided by Farouki (1981),  $x$  is the volume fraction in a unit soil volume.  $F_s$  is the ratio between the space average of the temperature gradient in the solid relative to the water phase, and  $F_a$  is the corresponding ratio for the thermal gradient in the air and water phases. Both  $F_s$  and  $F_a$  were computed from formulae presented by Farouki (1981).

Although some studies (e.g. Kane *et al.*, 2001) indicate that, under certain conditions, turbulent energy flows are important, others (e.g. Woo *et al.*, 2004; Roth and Boike, 2001, Romanovsky and Osterkamp, 2000) demonstrate that heat flow into the ground can be modelled effectively from conduction alone. The ground heat flux,  $Q_g$ , can be computed from (Fuchs, 1986):

$$Q_g = Q_s + Q_p + Q_i \quad (7)$$

where  $Q_s$ , the energy used to warm the active layer, was computed from:

$$Q_s = C_v (dT/dt)_j, \quad (8)$$

$Q_p$ , the energy used to warm the permafrost was computed from:

$$Q_p = \lambda (dT/dz), \quad (9)$$

and  $Q_i$ , the energy used to melt ice in the active layer, was computed from:

$$Q_i = \rho_{ice} \lambda f_1 (dh/dt). \quad (10)$$

In the above,  $dT/dt$  is the change in average soil temperature between successive days,  $j$  is the thickness of the zone of soil over which the computations were made,  $dT/dz$  is the temperature gradient between the deepest sensor in the active layer, and the sensor just below it, in permafrost,  $dh/dt$  is the rate that the top of the frozen saturated layer declines as the soil thaws ( $m d^{-1}$ ),  $f_1$  is the fractional ice content, and  $\rho_{ice}$  is the density of ice. Equations (2), (3) or (4) were used to compute  $C_v$ , and equations (5) or (6) to compute  $\lambda$ , depending on the state of the soil. A graduated steel rod was used for daily measurements of the depth of the impermeable frozen layer below the ground surface at the soil pit, needed to compute  $dh/dt$ . This simple method of directly measuring  $dh/dt$ , produced essentially the same results as  $dh/dt$  computed from the change in the position of the zero degree isotherm using soil temperature data.

Soil samples were collected from the middle of the upper and lower layers near (within 5 m) of the instrumented pit in order to determine the soil moisture response to variations in soil tension, and how this varied between the two layers. This information, needed in order to interpret variations in liquid moisture content with depth and time, was analysed using a pressure plate apparatus. Volumetric soil moisture was measured gravimetrically at nine increments of pressure head ranging between 0.001 (near saturation) to 5 m. Water retention characteristic curves were then fitted to the data using the approach of van Genuchten (1980). Because of the irreversible changes to the soil structure during sample drying, the procedure was not repeated for the wetting phase.

The late-winter maximum snow depth on the slope above the pit was measured in April 2002 and 2003 with an MSC snow sampler and calibrated scale. Net all-wave radiation ( $Q^*$ ), snow depth and rainfall were all measured at a meteorological tower, 10 m upslope of the pit.  $Q^*$  was measured 2 m above the ground surface, once it became snow-free on 23 May (2002) and 7 May (2003). Measurements were made with a REBS Q7 net radiometer every minute, averaged, and then recorded on a Campbell Scientific CR10X datalogger every half-hour. Lowering of the snow surface was monitored with an SR-50 sonic sensor with the same level of measurement. The accumulated rainfall in both years was measured with a shielded, tipping bucket rain gauge (Texas Instruments) every half hour.

In 2003, daily measurements of frost table depth were made with a graduated steel rod at 0.5 m intervals along a transect at nine snow-free patches on the hillslope. The patches chosen for measurement represent a variety of slope positions. Each snow-free patch was selected early in the melt period, and, initially was small, often less than a few metres in diameter. The measurement transect was oriented parallel to the hillslope, and as the snow-free area progressively increased, the transect length was increased to include new measurement points at 0.5 m increments. Eventually, the nine transects contained between 12 and 39 measurement points.

## RESULTS AND DISCUSSION

### Subsurface Water Movement

Soil samples taken from the face of the pit indicate that, with increasing depth, total porosity decreased, and bulk density increased (Table 1). This reflects the increasing state of soil decomposition with depth. The results of the pressure plate analysis (Figure 1a)

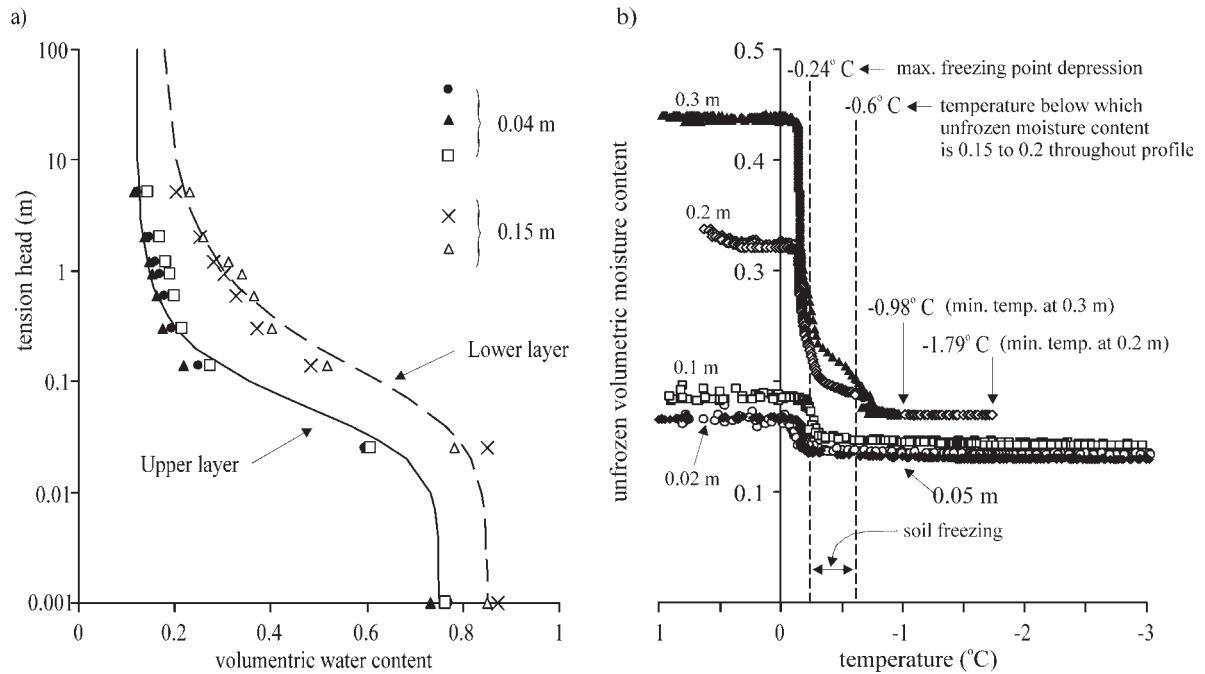


Figure 1 a) Variations in moisture content with tension during soil drying determined from pressure plate analysis on soils from the upper (0.04 m) and lower (0.15 m) organic layer sampled near the instrumented soil pit. The best fit curves were defined using the method of van Genuchten (1980). b) Variation in the unfrozen moisture content with soil temperatures measured every 30 min, 31 July to 31 December 2002.

indicate that, for a given level of tension, soils in the lower organic layer maintain a relatively high moisture content. Results also show that the two organic layers have a common residual moisture content of between 0.15 and 0.2 by volume. Figure 1b indicates that soils begin to freeze at temperatures slightly below  $0^{\circ}\text{C}$ . This freezing point depression varied between  $-0.14^{\circ}\text{C}$  and  $-0.24^{\circ}\text{C}$ . As soil temperatures drop below the freezing point depression, most of the reduction in the unfrozen moisture content occurred over a narrow temperature range of approximately  $0.15^{\circ}$  (Figure 1b). Over this temperature range, the unfrozen soil moisture per volume decreased by up to 0.05 in the upper layer and by *ca.* 0.2 in the lower layer. Regardless of the initial moisture content prior to freezing, the unfrozen moisture content fell to within 0.15 to 0.2 per volume once the soil temperature fell below *ca.*  $-0.6^{\circ}\text{C}$  (Figure 1b). This volume is approximately the same as the residual moisture content when the soil tension head increased to *ca.* 5 m (Figure 1a). In 2003, ground temperatures at all measurement points had lowered to the freezing-point

depression by 24 September, where they remained for a period of *ca.* 15 days in the upper layer (0.02, 0.05 and 0.10 m depths) and between 35 (0.20 m) and 55 (0.30 m) days in the lower layer (Figure 2). In the mineral sediment, temperature remained at the freezing point depression for 68 days. With increasing depth, the greater period of time that the soil temperature remained at the freezing-point depression in part reflects the increased moisture content with depth prior to the onset of freezing. Therefore, with increasing depth, more latent energy was released to offset the freezing process. Based on the difference in unfrozen moisture content before and after freezing at each depth, the latent energy released at 0.3 m was about five times greater than at 0.1 m.

The volumetric moisture content during the summer period was typically *ca.* 0.20 in the upper, and 0.40 in the lower organic layer (Figure 3), corresponding to soil tensions of approximately 0.3 m for both layers (Figure 1a). During winter, the unfrozen volumetric moisture content was close to 0.2 throughout the profile, as predicted from Figure 1b, which shows



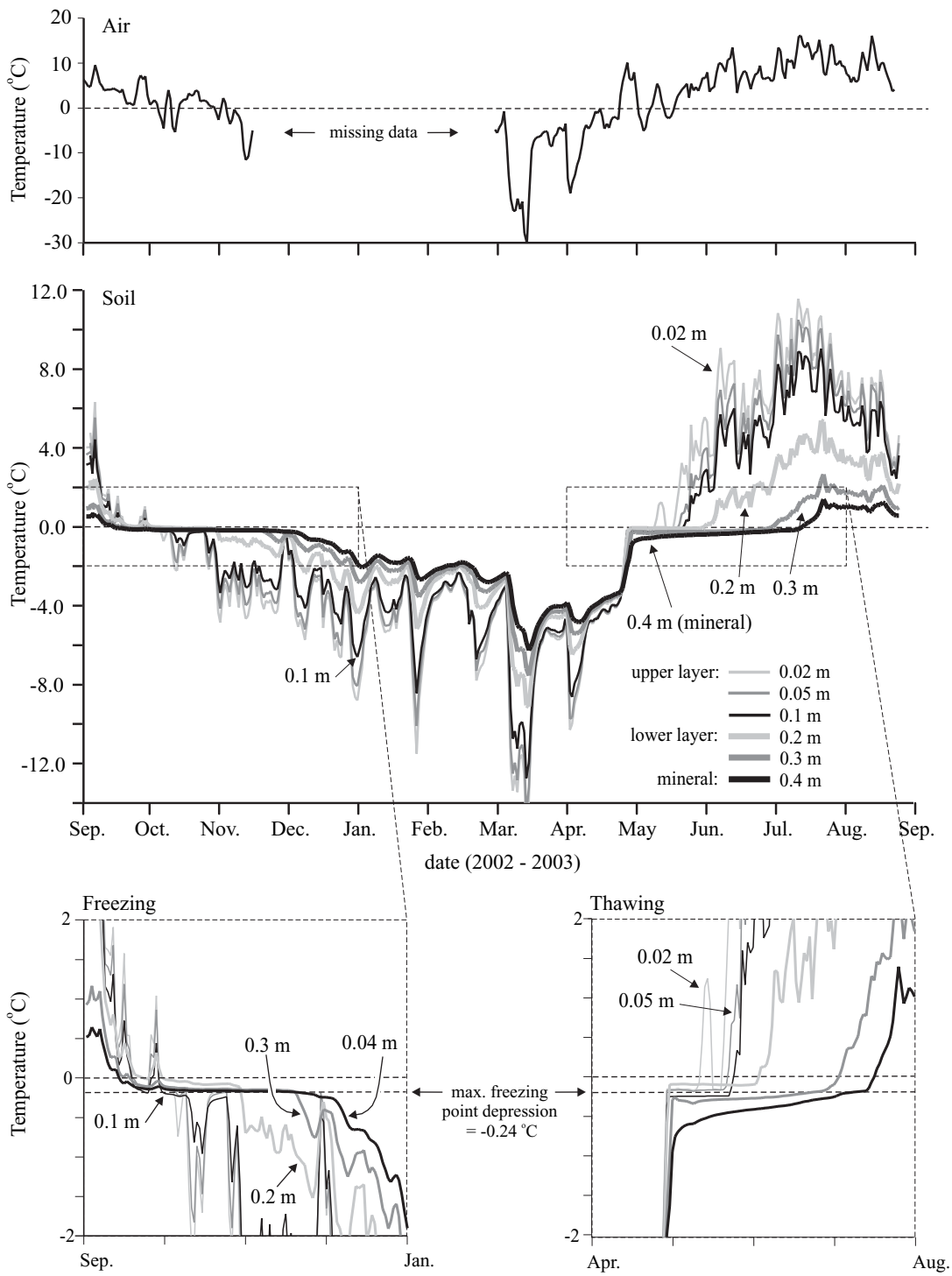


Figure 2 Variations in air and soil temperature at the instrumented pit, 1 September 2002 to 31 August 2003. Enlargements show soil temperature variations during soil freezing and thawing. Average daily values are used for graphing.

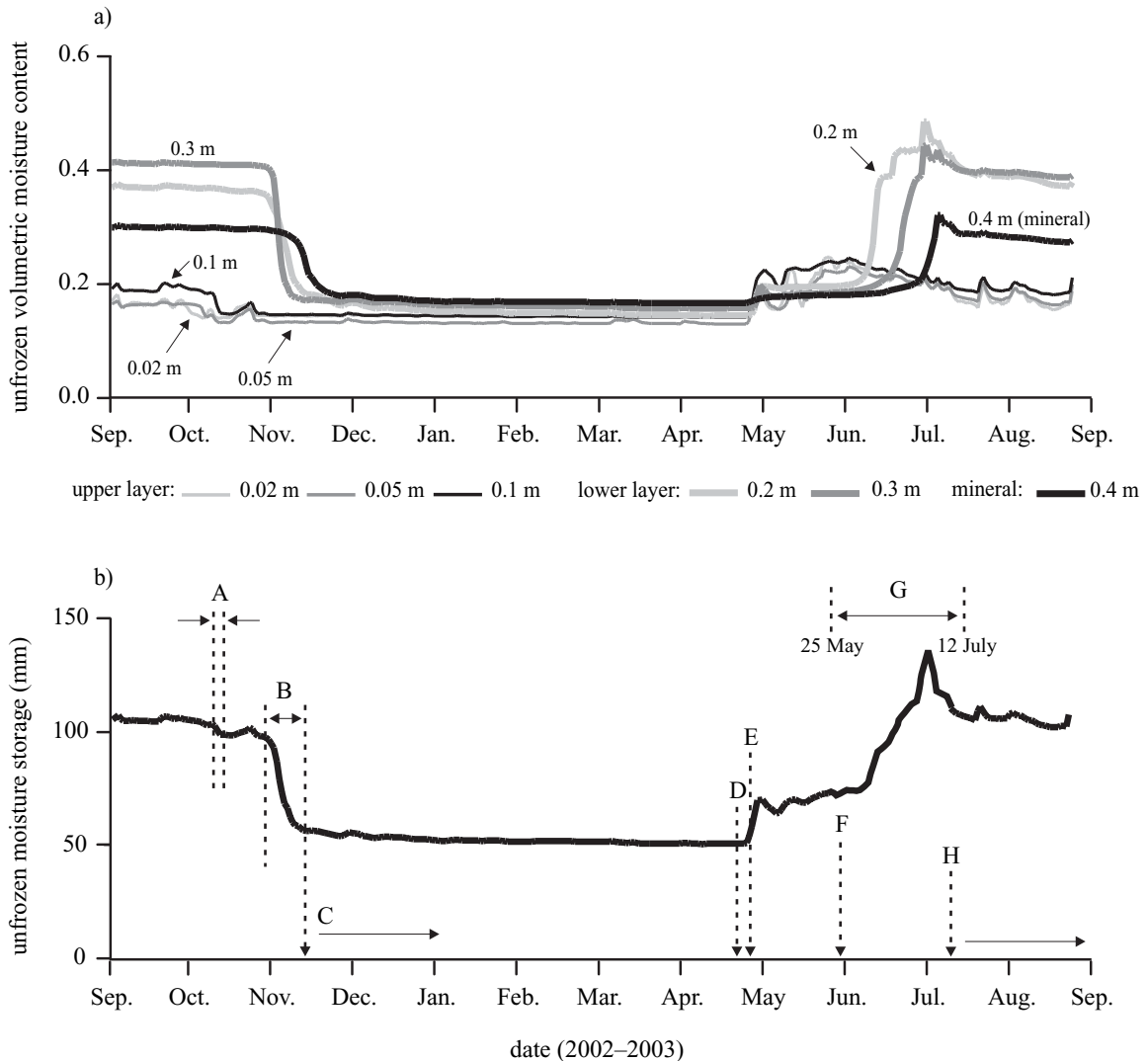


Figure 3 a) Variation in the unfrozen soil moisture content at the instrumented pit, 1 September 2002 to 31 August 2003. b) Total unfrozen moisture storage of the organic portion (0–0.35 m) of the instrumented pit, 1 September 2002 to 31 August 2003. A: soil temperature in upper layer reduces from freezing point depression (FPD) to  $-0.6^{\circ}\text{C}$  during 9–13 October; B: soil temperature in lower layer reduces from the FPD to  $-0.6^{\circ}\text{C}$  during 30 October–12 November; C: soil temperature  $< -0.6^{\circ}\text{C}$  and unfrozen volumetric moisture between 0.15 and 0.2 in both organic layers for the period 12 November 2002–26 April 2003; D: snow melt began 23 April; E: pit became snow-free on 29 April; F: soil temperature in lower layer rose above the FPD on 30 May; G: water table within organic soil; H: frost table within mineral sediment after 8 July.

that below a temperature of approximately  $-0.6^{\circ}\text{C}$ , the unfrozen moisture content throughout the profile converged to within 0.15 to 0.2 by volume. This also suggests a soil tension of *ca.* 5 m throughout the profile during winter (Figure 1a). The adjustment from summer to winter unfrozen moisture values

occurred while soil temperature decreased from the freezing point depression to *ca.*  $-0.6^{\circ}\text{C}$ . In the upper layer this happened relatively quickly, commencing on 9 October and lasting for only 4 days. In the lower layer, the freezing process began on 30 October and lasted 12 days. In the mineral sediment (0.40 m),

freezing began on 4 November and continued for 21 days.

In 2003, snowmelt began during the 8-day period of 23–30 April when air temperatures remained above 0°C (Figure 2). Ground temperatures at all measurement depths began to warm on 24 April, and reached the freezing-point depression temperature in the organic soil in the period 26–28 April. Although the 0.40 m deep (*ca.* 100 mm water equivalent) snow pack above the pit had melted by 29 April, appreciable ground warming was delayed owing to a return to colder air temperatures (Figure 2). Ground temperatures began to rise above 0°C between 18 May near the surface (0.02 m) and 12 July at depth (0.40 m). At each measurement depth, the unfrozen volumetric moisture content first rose above winter values in the period 25–27 May, when the soil pit was still below a melting snow cover, and when soil temperatures were increasing toward the freezing-point depression. Although soil temperatures in the upper layer (0.02, 0.05, 0.10 m) were relatively stable between 28 April and 18 May, Figure 3a indicates moisture fluctuations, the magnitude of which are only slightly larger than what occur when soil temperatures are close to the freezing-point depression (Figure 1b).

During winter, when soil temperatures are below -0.6°C, the total unfrozen moisture stored in the two organic layers is relatively constant at *ca.* 50 mm (Figure 3b). Following thaw of the upper layer, the unfrozen moisture storage rose to *ca.* 70 mm, and then to *ca.* 100 mm when the lower layer thawed (Figure 3b). This adjustment between storage levels occurred relatively quickly as soil temperatures rose above the freezing point depression (Figure 3b). A thawed, saturated layer, a zone that allows lateral subsurface drainage, was present in the organic soil between 25 May and 12 July, during which time the maximum moisture storage occurred (Figure 3b). It was also during this period that the organic soil transmitted water laterally downslope. However, this function began to change once soil thaw extended into the mineral sediment on 8 July. Once the water table (*i.e.* top of the thawed, saturated layer) also moved into the mineral sediment 4 days later, the hydrological role of the organic soil changed from one of lateral subsurface flow conveyance, to one of vertical water transmission from the ground surface, through the unsaturated organic soil, to the underlying mineral layer. Given the relatively high infiltration rates measured in the mineral sediment, it is unlikely that lateral drainage over the mineral interface is an important process. The analysis of temperature and moisture variations in the pit for the preceding year (Sept. 2001–Sept. 2002) produced similar results.

## Subsurface Energy Balance

The upper surface of the frozen, saturated zone began to descend on 17 May 2003, and by 8 July had reached the bottom of the organic layer 0.35 m below the ground surface. During this 52-day period, approximately 114 MJ m<sup>-2</sup> had entered the ground (Figure 4). Over this period, Qi (76%) and Qp (21%) consumed most ground heat flux, while Qs was a relatively minor component (3%). In the previous year, the organic soil took 49 days to thaw. Of the 105 MJ m<sup>-2</sup> that entered the ground in that period, Qi consumed 82%, Qp 15% and Qs 3%. The difference between the 2 years largely reflects inter-annual variations in soil moisture (water and ice) content. In both years, the cumulative ground heat flux ( $\Sigma Q_g$ ) was approximately 20% of the cumulative net all-wave radiation ( $\Sigma Q^*$ ) measured over the ground surface for the same period. Similar values were reported in other organic-covered, permafrost terrains (*e.g.* N. T. Roulet, unpublished PhD dissertation, 1985; Halliwell and Rouse, 1987). The cumulative Qi was approximately 15% of  $\Sigma Q^*$ .

Net radiation measurements from the snow-free mast are considered representative of the snow-free portions of the slope because slope angle varies within 5° of the mean of 20°, and both sky view and albedo are reasonably uniform over the hillslope (Pomeroy *et al.*, 2003). The small-scale variation of cumulative net radiation over this slope is overwhelmingly controlled by the timing of snowcover disappearance. It was estimated at points remote from the meteorological tower, but on the same slope angle, by summing net radiation from the snow-free tower over the time period that the point of interest was snow-free.

Measurements at the pit (Figure 4) provide an estimate of the ground heat flux and the subsurface partitioning of energy at a point. However, these fluxes must vary over the hillslope, since snow-cover duration, soil moisture (water and ice) content, and other factors vary widely (Carey and Woo, 2000). For example, an oblique photo of the study slope shows a snow-free patch (Patch 9) that was able to expand relatively rapidly because it was surrounded by shallow snow (Figure 5). Consequently, the increase in the average frost table depth over time was relatively gradual at Patch 9, because numerous new points, that recently had become snow-free and therefore had shallow thaw depths, were included in the average. Patches adjacent to deep, late-lying snow (*e.g.* Patch 8) expanded slowly and their patch-average frost-table depth increased more quickly.

The frost table in the pit lowered at a rate similar to the average rate at which it lowered in several snow-



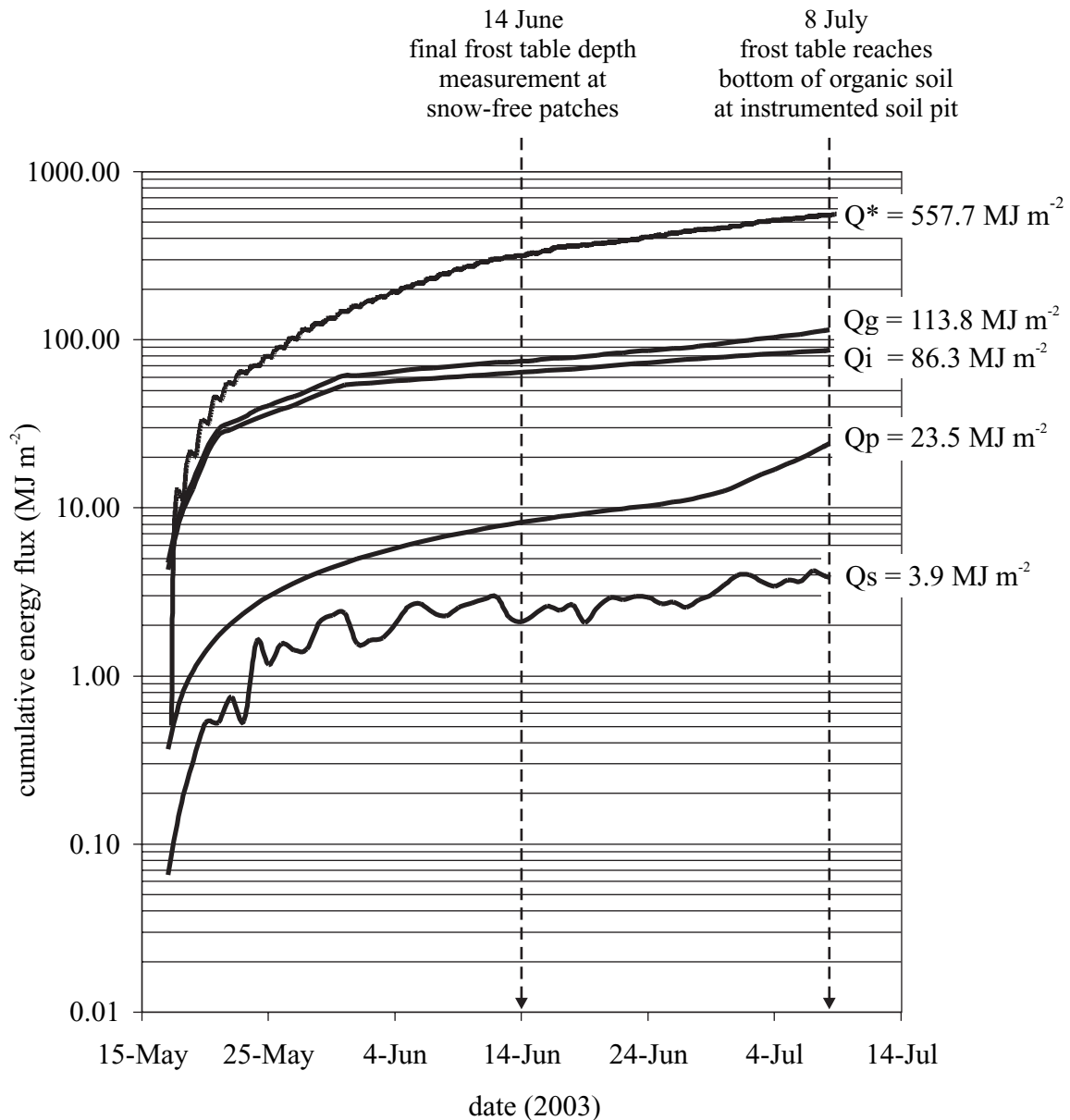


Figure 4 Graph showing the cumulative heat flux into the ground ( $Q_g$ ) at the instrumented pit for the period (17 May–8 July 2003) that was required to lower the frost table from the ground surface to the bottom of the organic soil. The cumulative portions of this flux used to melt ice in the active layer ( $Q_i$ ), warm the active layer ( $Q_s$ ), and warm the underlying permafrost ( $Q_p$ ) are also plotted, as is the cumulative net all-wave radiation ( $\Sigma Q^*$ ) measured at the meteorological tower.

free patches during the first half of the thaw period (Figure 6). However, with the exception of Patch 9 near the bottom of the slope, (where the average thickness of the organic soil was similar to that at the soil pit) the organic soil thickness in the other patches was  $<0.2$  m. Because the underlying mineral sediment had lower porosity and a lower moisture

content at saturation than the overlying organic soil, less energy was needed to thaw the sediment. Therefore, as the frost table descended below the relatively thin organic soil, the rate of thaw increased with time. For each patch, the cumulative amount of energy consumed in lowering the position of the frost table ( $\Sigma Q_i$ ) was computed using the same method used to

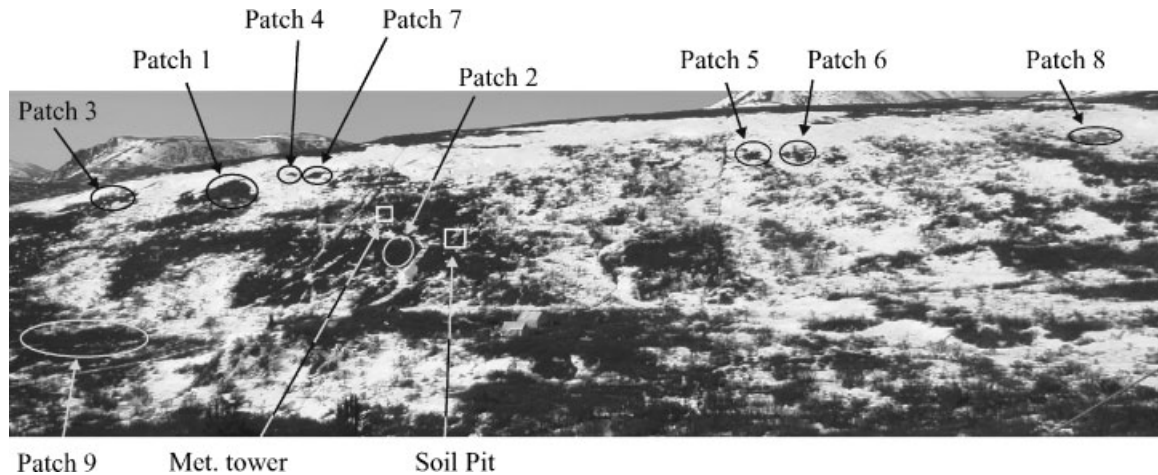


Figure 5 The north-facing study slope near the outlet of Granger Creek, Yukon, Canada. Photograph taken 1 May 2003. It shows the locations of the nine snow-free patches, the instrumented pit and the meteorological tower. The distance between patches 3 and 8 is *ca.* 380 m.

compute  $Q_i$  at the instrumented pit.  $\Sigma Q_i$  is plotted for each patch in Figure 7, along with the  $\Sigma Q^*$  that occurred over the same period for each patch. On average, the  $\Sigma Q_i$  was 15% of  $\Sigma Q^*$ , as was observed at the instrumented soil pit. There was little variation among the patches, despite variation in  $\Sigma Q^*$  (Figure 7). The average  $\Sigma Q_i$  of the nine patches was  $48.7 \text{ MJ m}^{-2}$  (std. dev. =  $16.2 \text{ MJ m}^{-2}$ ), while the average  $\Sigma Q^*$  was  $320.7 \text{ MJ m}^{-2}$  (std. dev. =  $59.9 \text{ MJ m}^{-2}$ ). In comparison, the cumulative values of  $Q_i$  and  $Q^*$  at the instrumented pit (Figure 4) were *ca.* 63.0 and  $328.0 \text{ MJ m}^{-2}$  respectively, both of which are similar to the average cumulative values of the patches.

A plot of  $\Sigma Q^*$  and  $\Sigma Q_i$  for all average frost depth measurements shown in Figure 8 provides the relation:

$$\Sigma Q_i = 0.15 \Sigma Q^* - 3.15 \quad (11)$$

indicating a strong association between  $\Sigma Q^*$  and  $\Sigma Q_i$  ( $R^2 = 0.91$ ,  $p < 0.05$ ). This suggests that if: i) the initial depth of the top of the frozen, saturated layer is known at the time that the ground surface becomes free, and ii) the cumulative net-all wave radiation since that time is also known, then the depth to frost can be obtained by converting  $\Sigma Q_i$  from equation (8) into the equivalent cumulative depth of thaw  $dt$ ,

$$\Sigma dt = (\Sigma Q_i / \rho_i h_f) f_i \quad (12)$$

where  $Q_i$  is in units of  $\text{J m}^{-2}$ ,  $\rho_i$  is the density of ice,  $h_f$  is the latent heat of fusion, and  $f_i$  is the volume fraction of ice at the frost table. It is assumed that at the top of the frozen saturated layer,  $f_i$  is equivalent to

the porosity,  $\phi$ , minus the small amount (15–20%) of unfrozen water.

## CONCLUSIONS

This study examined the effects of ground freezing and thawing on the liquid moisture content of the organic soil in the active layer. Results indicate that ground freezing and thawing are initiated within a narrow temperature range of  $-0.14$  to  $-0.24^\circ\text{C}$ , and that a further decrease below  $-0.6^\circ\text{C}$  has little effect on unfrozen moisture content. Throughout most of the year, variations in unfrozen moisture storage occur in the absence of a horizontal flux. The exception is the initial thaw period when an unfrozen saturated layer occurs within the organic soil. It is during such a period that soil moisture storage is affected by horizontal flow conveyance. After the water table subsides into the underlying mineral sediment, organic soil moisture storage is controlled by vertical fluxes, including the transfer of moisture from the ground surface to the mineral sediment. At the instrumented pit, the  $\Sigma Q_i$  in the active layer was *ca.* 76% of the cumulative ground heat flux ( $\Sigma Q_g$ ), and *ca.* 15% of the  $\Sigma Q^*$ . For nine snow-free patches, the average amount of energy used to melt ice in the active layer was also *ca.* 15% of the  $\Sigma Q^*$ . A strong linear correlation between  $\Sigma Q^*$  and  $\Sigma Q_i$ , suggests that the elevation of the frost table, needed to model subsurface horizontal drainage, can be estimated simply from the  $\Sigma Q^*$  measured at the ground surface from the time it becomes snow-free.

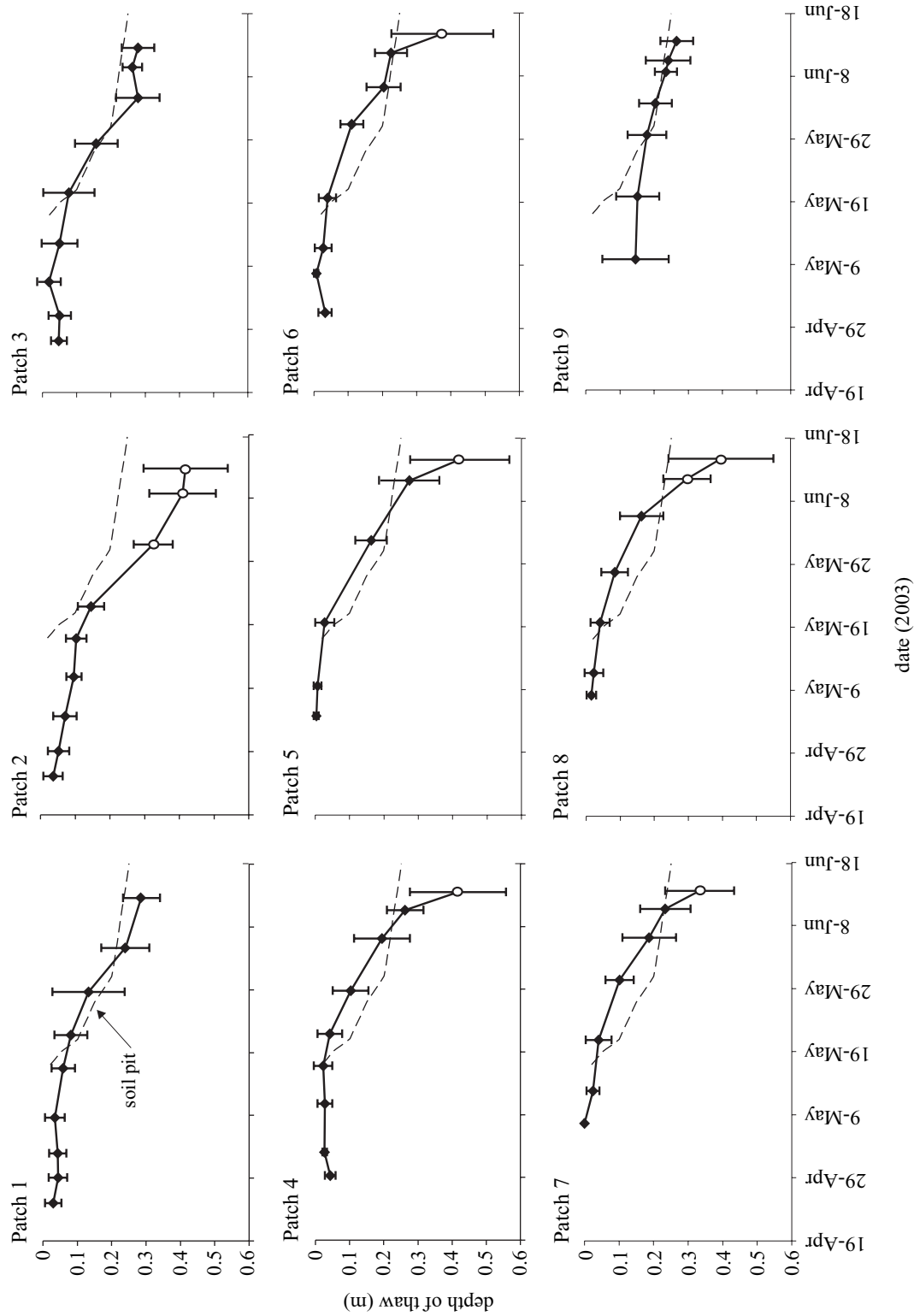


Figure 6 The thaw rate measured at the instrumented pit (dashed line) plotted together with average thaw rate measured at each snow-free patch for the period when the frost table depth was measured at the patches. Data points represent the mean frost table depth, and bars represent one standard deviation above and below the mean depth for that day. Open symbols indicate the frost table was below the organic layer at >50% of the measurement points in the transect, otherwise a solid symbol is displayed.

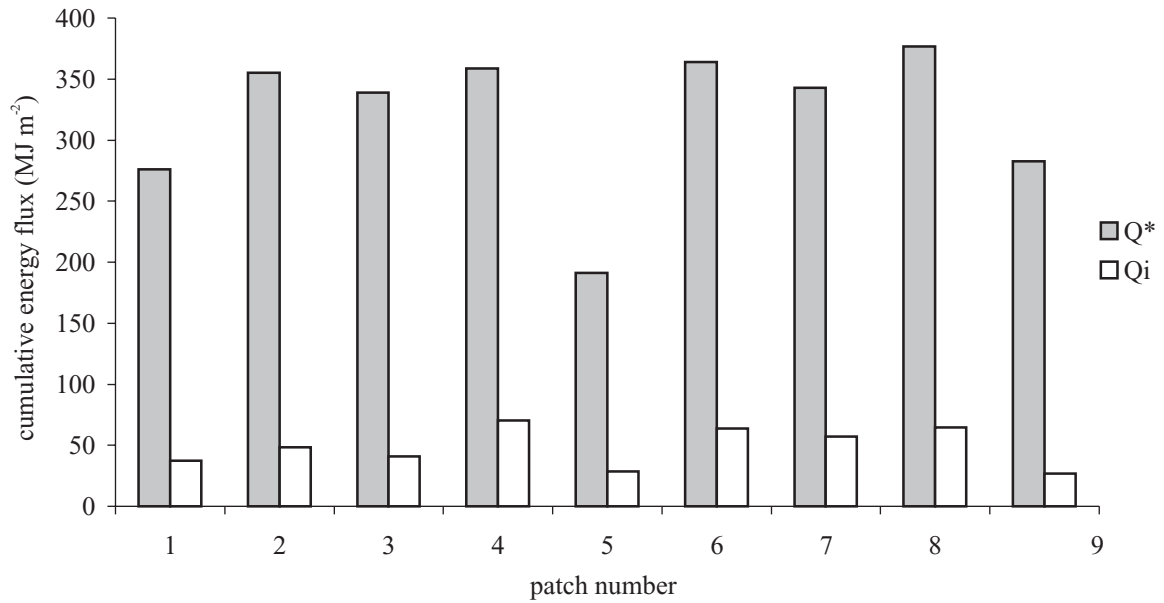


Figure 7 Graph showing cumulative net all-wave radiation ( $\Sigma Q^*$ ) and cumulative energy used to melt ice (i.e. lower the frost table) in the active layer ( $\Sigma Q_i$ ) during thaw in 2003, from the time of initial frost depth measurement when bare ground first appeared at each patch, until the final day of frost depth measurement. Variations in  $\Sigma Q^*$  among the patches occurred because snow-free patches developed at different times.

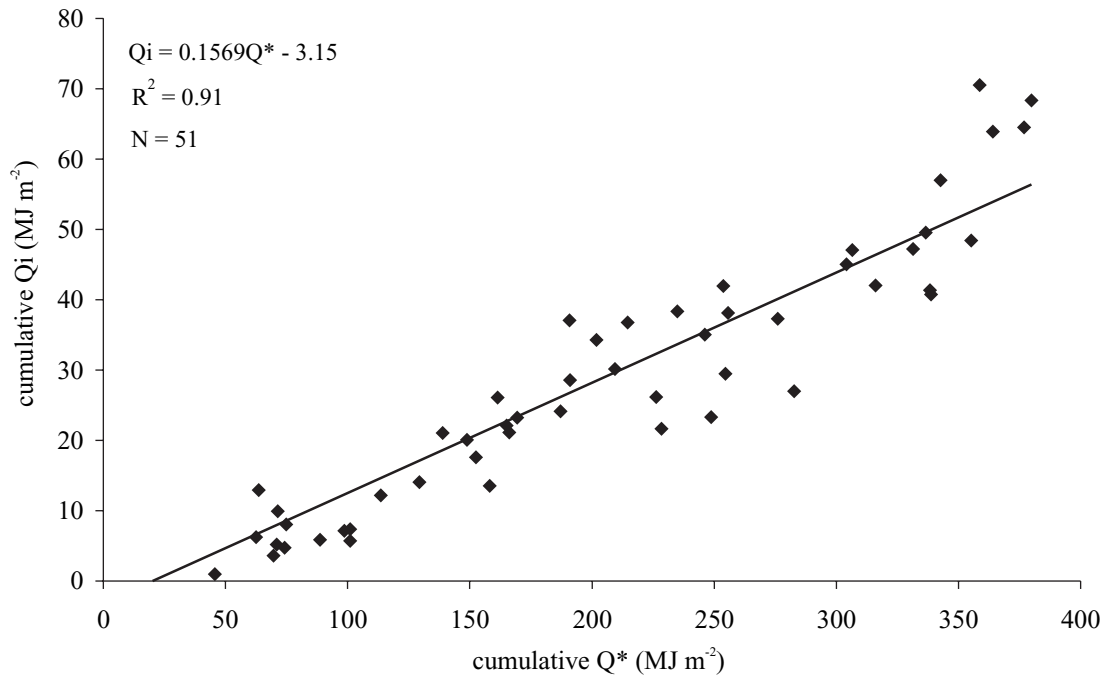


Figure 8 Plot of cumulative energy used to melt ice in the active layer ( $\Sigma Q_i$ ) (computed from the average frost table depth measurements presented in Figure 6) and cumulative net all-wave radiation ( $\Sigma Q^*$ ) over the same period.

## ACKNOWLEDGEMENTS

The authors wish to thank the two anonymous referees for their many helpful comments and suggestions. We also wish to thank Steve McCartney and Chris deBeer for their assistance in the field, Claire Kaufman for her assistance with data preparation and image analysis, and Dr M. Hayashi for conducting the pressure-plate analysis on soil samples at the University of Calgary. Glen Ford and Ric Janowicz of the Department of Indian and Northern Affairs and Newell Hedstrom and Raoul Granger of Environment Canada kindly provided logistical assistance during the field study. This research was funded by the Natural Science and Engineering Research Council of Canada (NSERC), the Natural Environment Research Council of the United Kingdom (NERC), and by the Canadian Foundation for Climate and Atmospheric Sciences (CFCAS).

## REFERENCES

- Andersland OB, Ladanyi B. 1994. Physical and thermal properties. In *An Introduction to Frozen Ground Engineering*. Chapman and Hall: New York; 1–62.
- Bliss LC, Matveyeva NV. 1992. Circumpolar arctic vegetation. In *Arctic Ecosystems in a Changing Climate: An Ecological Perspective*, Chapin FS, Jefferies RL, Reynolds JF, Shaver GR, Svoboda J (eds). Academic Press: San Diego; 59–89.
- Boelter DH. 1972. Watertable drawdown around an open ditch in organic soils. *Journal of Hydrology* **15**: 329–340.
- Bouwer H. 1989. The bouwer and rice slug test—an update. *Ground Water* **27**: 304–309.
- Carey SK, Quinton WL. 2005. Evaluating runoff generation during summer using hydrometric, stable isotope and hydrochemical methods in a discontinuous permafrost alpine catchment. *Hydrological Processes* **19**: 95–114. DOI: 10.1002/hyp.5764.
- Carey SK, Woo MK. 1998. Snowmelt hydrology of two subarctic slopes, southern Yukon, Canada. *Nordic Hydrology* **29**: 331–346.
- Carey SK, Woo MK. 2000. Within slope variability of ground heat flux, subarctic Yukon. *Physical Geography* **21**: 407–417.
- Carey SK, Woo MK. 2001. Slope runoff processes and flow generation in a subarctic, subalpine environment. *Journal of Hydrology* **253**: 110–129.
- Comiso JC, Parkinson CL. 2004. Satellite-observed changes in the arctic. *Physics Today* **57**: 38–44.
- Farouki OT. 1981. The thermal properties of soils in cold regions. *Cold Regions Science and Technology* **5**: 61–74.
- Fuchs M. 1986. Heat flux. In *Methods of Soil Analysis, Part 1, Physical and Mineralogical Methods*, 2nd edn, Klute A (ed.). Soil Science Society of America: Madison, Wisconsin; 957–968.
- Granger RJ, Pomeroy JW. 1997. Sustainability of the western Canadian boreal forest under changing hydrological conditions—summer energy and water use. In *Sustainability of Water Resources under Increasing Uncertainty*, Rosjberg D, Boutayeb N, Gustard A, Kundzewicz Z, Rasmussen P (eds). IAHS Publication No. 240. IAHS Press: Wallingford, UK; 243–250.
- Gray DM, Toth B, Zhao L, Pomeroy J, Granger R. 2001. Estimating areal snowmelt infiltration into frozen soils. *Hydrological Processes* **15**: 3095–3111.
- Halliwel DH, Rouse WR. 1987. Soil heat flux in permafrost: characteristics and accuracy of measurement. *Journal of Climatology* **7**: 571–584.
- Hayashi M, Quinton WL, Pietroniro A, Gibson J. 2004. Hydrologic functions of wetlands in a discontinuous permafrost basin indicated by isotopic and chemical signatures. *Journal of Hydrology* **296**: 81–97.
- Intergovernmental Panel on Climate Change (IPCC). 1996. Impacts, adaptations and mitigation of climate change: scientific-technical analyses. In *World Meteorological Organisation, Contribution of Working Group II to the Second Assessment Report of the Intergovernmental Panel on Climate Change*, Watson RT, Zonary LC, Moss RL (eds). Cambridge University Press: Cambridge, UK; 879.
- Janowicz RJ, Gray DM, Pomeroy JW. 2003. Spatial variability of fall soil moisture and spring snow water equivalent within a mountainous sub-arctic watershed. *Proceedings of the Eastern Snow Conference* **60**: 127–139.
- Kane DL, Hinkel KM, Goering DJ, Hinzman LD, Outcalt SI. 2001. Non-conductive heat transfer associated with frozen soils. *Global and Planetary Change* **29**: 275–292.
- Oke TR. 1987. *Boundary Layer Climates*. Methuen: London; 356.
- Pomeroy JW, Granger RJ. 1999. *Wolf Creek Research Basin: Hydrology, Ecology, Environment*. National Water Research Institute: Environment Canada; 160.
- Pomeroy JW, Toth B, Granger RJ, Hedstrom NR, Essery RLH. 2003. Variation in surface energetics during snowmelt in a subarctic mountain catchment. *Journal of Hydrometeorology* **4**: 702–719.
- Quinton WL, Marsh P. 1999. A conceptual framework for runoff generation in a permafrost environment. *Hydrological Processes* **13**: 2563–2581. DOI: 10.1002/hyp.1369.
- Quinton WL, Gray DM. 2001. Estimating subsurface drainage from organic-covered hillslopes underlain by permafrost: toward a combined heat and mass flux model. Soil-vegetation-atmosphere transfer schemes and large-scale hydrological models. Sixth IAHS Scientific Assembly, Maastricht, Netherlands; 333–341.



- Quinton WL, Gray DM. 2003. Subsurface drainage from organic soils in permafrost terrain: the major factors to be represented in a runoff model. In *Proceedings of the 8th International Conference on Permafrost, Zurich, Switzerland*, Phillips M, Springman SM, Arenson LU (eds). Balkema: Lisse; 1380.
- Quinton WL, Gray DM, Marsh P. 2000. Subsurface drainage from hummock-covered hillslopes in the Arctic tundra. *Journal of Hydrology* **237**: 113–125.
- Quinton WL, Carey SK, Goeller NT, Pomeroy JW. 2004. Snowmelt runoff from northern alpine tundra hillslopes: major processes and methods of simulation. *Hydrology and Earth System Sciences* **8**: 877–890.
- Romanovsky VE, Osterkamp TE. 2000. Effects of unfrozen water on heat and mass transport in the active layer and permafrost. *Permafrost and Periglacial Processes* **11**: 219–239. DOI: 10.1002/1099–1530.
- Roth K, Boike J. 2001. Quantifying the thermal dynamics of a permafrost site near Ny-Alesund, Svalbard. *Water Resources Research* **37**: 2901–2914.
- Roulet NT. 1985. Runoff hydrology of a low arctic drainage basin. Unpublished Ph.D. Thesis, McMaster University, 166pp.
- Seyfried MS, Murdock MD. 2001. Response of a new soil water sensor to variable soil, water content, and temperature. *Soil Science Society of America Journal* **65**: 28–34.
- Spence C, Woo MK. 2003. Hydrology of subarctic Canadian shield: soil-filled valleys. *Journal of Hydrology* **279**: 151–166.
- van Genuchten MT. 1980. A closed-form equation for predicting the hydraulic conductivity of unsaturated soils. *Soil Science Society of America Journal* **44**: 892–898.
- Woo M-K, Arain MA, Mollinga M, Yi S. 2004. A two-directional freeze and thaw algorithm for hydrologic and land surface modelling. *Geophysical Research Letters* **31**: L12501. DOI: 10.1029/2004GL019475.